Manuscript prepared for Atmos. Chem. Phys.
with version 5.0 of the LaTeX class copernicus.cls.
Date: 26 June 2014

OH regeneration from methacrolein oxidation investigated in the atmosphere simulation chamber SAPHIR

H. Fuchs[1], I.-H. Acir[1], B. Bohn[1], T. Brauers[1], H.-P. Dorn[1], R. Häseler[1],
A. Hofzumahaus[1], F. Holland[1], M. Kaminski[1], X. Li[1], K. Lu[1,*], A. Lutz[2],
S. Nehr[1,**], F. Rohrer[1], R. Tillmann[1], R. Wegener[1], and A. Wahner[1]

[1]Institute of Energy and Climate Research, IEK-8: Troposphere, Forschungszentrum Jülich GmbH, Jülich, Germany
[2]Institute of Chemistry and molecular Biology, Göteborg University, Göteborg, Sweden
[*]now at: College of Environmental Sciences and Engineering, Peking University, Beijing, China
[**]now at: Verein Deutscher Ingenieure e.V., Kommission Reinhaltung der Luft, Düsseldorf, Germany

Correspondence to: Hendrik Fuchs
(h.fuchs@fz-juelich.de)

Abstract. Hydroxyl radicals (OH) are the most important reagent for the oxidation of trace gases in the atmosphere. OH concentrations measured during recent field campaigns in isoprene rich environments were unexpectedly large. A number of studies showed that unimolecular reactions of organic peroxy radicals ($\mathrm{RO_2}$) formed in the initial reaction step of isoprene with OH play an important role for the OH budget in the atmosphere at low mixing ratios of nitrogen monoxide (NO) of less than 100 pptv. It has also been suggested that similar reactions potentially play an important role for $\mathrm{RO_2}$ from other compounds. Here, we investigate the oxidation of methacrolein (MACR), one major oxidation product of isoprene, by OH in experiments in the simulation chamber SAPHIR under controlled atmospheric conditions. The experiments show that measured OH concentrations are approximately 50 % larger than calculated by the Master Chemical Mechanism (MCM) for conditions of the experiments (NO mixing ratio of 90 pptv). The analysis of the OH budget reveals an OH source that is not accounted for in MCM, which is correlated with the production rate of $\mathrm{RO_2}$ radicals from MACR. In order to balance the measured OH destruction rate, 0.77 OH radicals (1σ error: ± 0.31) need to be additionally reformed from each reaction of OH with MACR. The strong correlation of the missing OH source with the production of $\mathrm{RO_2}$ radicals is consistent with the concept of OH formation from unimolecular isomerization and decomposition reactions of $\mathrm{RO_2}$. The comparison of observations with model calculations gives a lower limit of $0.03\,\mathrm{s^{-1}}$ for the reaction rate constant, if the OH source is attributed to an isomerization reaction of $\mathrm{MACR{-}1{-}OH{-}2{-}OO}$ and $\mathrm{MACR{-}2{-}OH{-}2{-}OO}$ formed in the MACR+OH reaction as suggested in literature (Crounse et al., 2012). This fast isomerization reaction would be competitive to

the reaction of this $\mathrm{RO_2}$ species with minimum $150\,\mathrm{pptv}$ NO. The isomerization reaction would be the dominant reaction pathway for this specific $\mathrm{RO_2}$ radical in forested regions, where NO mixing ratios are typically much smaller.

1 Introduction

Isoprene (2-methyl-1,3-butadiene) is the most abundant nonmethane hydrocarbon that is being emitted by the biosphere and predominantly removed by oxidation with atmospheric hydroxyl radicals (OH) (Guenther et al., 2012). Unexpectedly large OH concentrations that cannot be explained by the current knowledge of atmospheric chemistry have been found in several field campaigns (Carslaw et al., 2001; Tan et al., 2001; Kuhn et al., 2007; Ren et al., 2008; Lelieveld et al., 2008; Hofzumahaus et al., 2009; Lu et al., 2012, 2013; Stone et al., 2010; Whalley et al., 2011; Wolfe et al., 2011) for high loads of OH reactants (often dominated by isoprene) and low concentrations of nitrogen monoxide (NO). As a potential explanation for the high OH concentrations, reformation of OH radicals from unimolecular reactions of organic peroxy radicals ($\mathrm{RO_2}$) that result from the reaction of isoprene with OH have been suggested (Peeters et al., 2009; Peeters and Müller, 2010; da Silva et al., 2010). The proposed reactions involve 1,5-H- and 1,6-H-shift reactions followed by decomposition of specific isoprene $\mathrm{RO_2}$ isomers and compete with the well-known OH reformation via reaction of $\mathrm{HO_2}$ with NO. This reaction scheme has been applied, in order to explain high levels of OH radicals, using reaction rate constants that were derived from quantum chemical calculations (Peeters et al., 2009; Taraborrelli et al., 2012). A laboratory study investigated the product yields of the proposed reactions (Crounse et al., 2011; Wolfe et al., 2012) and direct OH measurements in experiments in the atmosphere simulation chamber SAPHIR gave evidence for OH regeneration from isoprene $\mathrm{RO_2}$ without involvement of NO (Fuchs et al., 2013). Results from these experimental studies are consistent with the $\mathrm{RO_2}$ isomerization reaction scheme, but also showed that isomerization reaction rate constants are smaller than e.g. those calculated by Peeters and Müller (2010). Thus, OH regeneration from isoprene peroxy radicals alone cannot explain elevated OH concentrations found in field campaigns. Therefore, the question arises, if unimolecular $\mathrm{RO_2}$ reactions from the oxidation products of isoprene may also enhance atmospheric OH.

Methacrolein (2-methylpropenal) is one of the major first-generation products of the gas-phase oxidation of isoprene by OH with a yield of approximately 20–30 % for atmospheric conditions (Tuazon and Atkinson, 1990; Galloway et al., 2011; Liu et al., 2013). Methacrolein (MACR) is further oxidized by OH in the atmosphere producing hydroxyacetone, methylglyoxal, and formaldehyde (Galloway et al., 2011). Similar unimolecular reactions of $\mathrm{RO_2}$ as for isoprene, which may produce additional OH, have also been suggested for MACR (Peeters et al., 2009; Crounse et al., 2012; Asatryan et al., 2010; da Silva, 2012). Recently, the product distribution from the MACR plus OH reaction for various NO concentrations has been investigated in a laboratory study accompanied by quantum chemical calculations (Crounse et al., 2012). They inferred a new reaction pathway, in which hydroxyacetone is formed independently of the level of NO. This would be consistent with a fast unimolecular $\mathrm{RO_2}$ reaction, because hydroxyacetone has so far only been known as a product of the reaction of $\mathrm{RO_2}$ with NO. The new reaction path is attributed to a 1,4-H-shift isomerization reaction with concurrent reformation of OH confirmed by isotopic measurements reported in the work by Crounse et al. (2012).

Here, we present the investigation of the photo-oxidation of MACR by OH at controlled atmospheric conditions in the simulation chamber SAPHIR in the presence of approximately $90\,\mathrm{pptv}$ NO. Measurements allow a detailed analysis of the OH budget. Recently proposed reaction pathways are tested by comparing time series of measurements with model calculations.

2 Methods

2.1 Simulation experiment in SAPHIR

Experiments were conducted in the atmosphere simulation chamber SAPHIR in Jülich, Germany. The chamber allows to investigate the photochemical oxidation of organic compounds at atmospheric conditions with respect to temperature, pressure, radiation and concentrations of trace gases and radicals. Experiments for this study were similar to those that were performed to investigate the oxidation of isoprene by OH (Fuchs et al., 2013).

The outdoor SAPHIR chamber is made of a double wall Teflon (FEP) film of cylindrical shape (length $18\,\mathrm{m}$, diameter $5\,\mathrm{m}$, volume $270\,\mathrm{m}^3$). Details of the chamber have been described earlier (Rohrer et al., 2005; Bohn et al., 2005; Schlosser et al., 2009). It is equipped with a shutter system, which can be opened to expose the chamber air to natural sunlight. The FEP film has a high transmittance for the entire spectrum of solar radiation (Bohn et al., 2005). Slight overpressure prevents leakage of ambient air into the chamber. The chamber air is mixed from evaporated liquid nitrogen and oxygen of highest purity (Linde, purity $> 99.99990\,\%$). During all experiments reported here, a fan ensured fast mixing of the chamber air (mixing time $< 2\,\mathrm{min}$). Replenishment of chamber air, which is lost due to small leakages and consumption by instruments, leads to a dilution of trace gases with a rate of approximately $4\,\%\,\mathrm{h}^{-1}$.

The chamber experiments aimed to simulate conditions like those found during several field experiments (Lu et al., 2012, 2013), when unexpectedly large OH concentrations were measured. At the beginning of the experiment, the dark chamber only contained clean synthetic air. The water vapour mixing ratio was increased by flushing water vapour from boiling Milli-Q®-water into the chamber in the dark, until the relative humidity reached approximately 80 %. Then the shutter system was opened to expose the chamber to sunlight. Ozone produced from a silent discharge ozoniser (O3Onia) was added resulting in a mixing ratio of approximately $50\,\mathrm{ppbv}$. The initial phase ("ZA") with zero air, water vapour, and ozone had a total duration of 2 hours. Thereafter, MACR was injected several times increasing the mixing ratio by $7\,\mathrm{ppbv}$ each time. The maximum mixing ratio was $14\,\mathrm{ppbv}$. The experiment was performed three times in a similar way (Table 1). On 11 August 2011 OH production rates from photolysis were highest and a large number of instruments was available. Therefore, time series and model calculations from this experiment are shown here. Experiments on the other two days give similar results and are included in the analysis of the OH budget.

The major primary source for OH in the chamber is photolysis of nitrous acid (HONO), which is released from the Teflon film depending on temperature, relative humidity, and strength of radiation (Rohrer et al., 2005). HONO photolysis is also the major source of nitrogen oxides. In addition, acetaldehyde and formaldehyde are formed with a rate of approximately 200 $\mathrm{pptv\,h^{-1}}$ during these experiments. The OH reactivity is on the order of (1–2) $\mathrm{s^{-1}}$ in the absence of additional OH reactants, which can be partly explained by the presence of NO, $\mathrm{NO_2}$, formaldehyde (HCHO) and acetaldehyde ($\mathrm{CH_3CHO}$). $\mathrm{RO_2}$ radicals of approximately $(1–2) \times 10^{8}\,\mathrm{cm^{-3}}$ were immediately formed in the humidified clean air when the chamber roof was opened. They were partly formed by photolytic processes. This is evident from reference experiments with CO, in which the $\mathrm{RO_2}$ radical concentrations persisted even though OH was completely scavenged by excess CO, so that no $\mathrm{RO_2}$ production is expected from the reaction of OH with organic compounds. Sources of trace gases and radicals can be well-parameterized from reference experiments, but except for the production of HONO they played only a minor role for the experiments after MACR had been injected.

2.2 Instrumentation

Trace gas and radical concentrations were measured by instruments listed in Table 2. A laser induced fluorescence instrument (LIF) was used to measure OH, $\mathrm{HO_2}$, and $\mathrm{RO_2}$ concentrations simultaneously in three parallel measurement cells. $\mathrm{RO_2}$ and $\mathrm{HO_2}$ are detected via their conversion to OH involving reactions with NO. The signal of the $\mathrm{HO_2}$ detection includes a small fraction of specific $\mathrm{RO_2}$ species, which can be partly converted to OH on the same time-scale (Fuchs et al., 2011). Instrument parameters were optimized to minimize this interference. For those $\mathrm{RO_2}$ where conversion to OH requires more than two reactions with NO (e.g. acyl peroxy radicals), the conversion efficiency is assumed to be small, because of the short residence time between NO addition and OH detection in the instrument (Fuchs et al., 2008). The measured detection efficiency for MACR derived $\mathrm{RO_2}$ is similar to that of methyl-peroxy radicals (i.e. they are converted to OH on the relevant timescales).

OH was also detected by a Differential Optical Absorption Spectrometer (DOAS) during two of the three experiments. As previously shown, measurements of both instruments (LIF and DOAS) usually agreed within their uncertainties during experiments in SAPHIR that were performed for the investigation of the oxidation of various organic compounds including MACR (Schlosser et al., 2007, 2009; Fuchs et al., 2012). This indicates that OH measurements were not affected by unknown interferences.

During the experiment on 11 August 2011, the OH measurements by DOAS were 0.5×10^{6} $\mathrm{cm^{-3}}$ lower than those measured by LIF; such a difference was not observed in other experiments investigating MACR oxidation (Fuchs et al., 2012). For the analysis of data from 11 August 2011 in Fig. 2 and 5, we chose the DOAS data, which is regarded to be an absolute measurement reference

(Schlosser et al., 2009).

The chemical lifetime of OH was measured applying a combination of flash photolysis producing OH by ozone photolysis at 266 nm in a reaction cell under slow-flow conditions and time-resolved detection of OH by LIF (Lou et al., 2010). The evaluation of the pseudo-first-order decays gives directly the rate coefficient of the OH loss (OH reactivity) or inverse OH lifetime. OH regeneration from subsequent chemistry can disturb measurements (Lou et al., 2010), but was not observed during these experiments, because OH was regenerated from RO_2 radicals on a much longer time scale (see below) compared to the time scale of the OH decay in the instrument.

Organic compounds were measured by a Proton-Transfer-Reaction-Time-Of-Flight Mass-Spectrometry instrument (PTR-TOF-MS), nitrogen oxides and ozone by chemiluminescence instruments and nitrous acid by a LOng Path Absorption Photometer (LOPAP). During one of the experiments, peroxyacyl nitrates, PAN and MPAN, which serve as reservoirs for peroxy radicals and nitrogen oxides during MACR oxidation, were detected by gas chromatography (GC).

2.3 Model calculations

Time series of measurements were compared to calculations using the Master Chemical Mechanism version 3.2 (MCM) (Jenkin et al., 1997; Saunders et al., 2003) available at http://mcm.leeds.ac.uk/MCM. Throughout the paper "MCM" denotes the mechanism in its current version 3.2. The MCM provides near-explicit mechanisms of the atmospheric degradation of organic compounds. In addition to the chemistry from the MCM, chamber specific properties were included in the model calculations. Dilution of trace gases due to the replenishment of zero air was modelled from monitored rates of the dilution flow. The dependence of source strengths for HONO, HCHO and CH_3CHO on radiation, relative humidity and temperature were taken from parameterizations described earlier (Rohrer et al., 2005; Karl et al., 2006). The source strengths were scaled, in order to match formation of NO_X, HCHO and CH_3CHO during the zero air part of the experiment. The part of the OH reactivity (approximately $1\,s^{-1}$) which could not be explained by the presence of measured OH reactants was treated as an OH reactant of constant concentration, which converts OH to HO_2 like CO does. The value of this "background" OH reactivity was determined from the measured OH reactivity at the start of the experiment (dark chamber), when only zero air and water vapour was present. Also RO_2 radicals were formed in the sunlit chamber from unknown sources. A photolytic RO_2 source was implemented in the model, which was similarly parameterized as the empirical functions for the HONO and HCHO sources. Test experiments with only humidified zero air in the chamber showed that RO_2 time series can be well described by this procedure. Effects on measurements during VOC oxidation experiments are small.

The model was constrained by measurements of temperature, pressure, calculated dilution rates, measured water vapour mixing ratios, and photolysis frequencies for NO_2, HCHO, O_3, MACR and HONO. Photolysis frequencies and relative humidity constrained the calculated chamber sources for

HONO, HCHO, and CH_3CHO. Photolysis frequencies that were not measured were first calculated by a MCM (version 3.1) function for clear sky conditions and then scaled by the ratio of the measured and calculated NO_2 photolysis frequencies to account for reductions of the solar radiation by clouds and the transmission of the Teflon film. Constrained parameters were re-initialized on a 1 min time grid. The injection of trace gases (O_3, MACR) was modelled as sources, which were turned on for the time of the injection. The source strength for ozone was adjusted to match the measured concentrations right after the injection and that for MACR was adjusted to match the change in the measured OH reactivity. Otherwise, trace gas concentrations were calculated by the model.

Modelled HO_2 concentrations presented here are the sum of calculated HO_2 and a fraction of specific RO_2 that are an interference in the HO_2 measurements (like introduced by Lu et al., 2012, as HO_2^*), so that measurements can be compared to calculations. Model calculations taking RO_2 conversion efficiency from characterization experiments of the instrument suggest that the contribution of this interference to the entire HO_2 detection was less than 5 % for these experiments, most of which is caused by RO_2 from MACR. Calculated RO_2 concentrations that are shown in the following only include those RO_2 species that are efficiently converted to OH in the RO_2 measurement channel of the LIF instrument.

3 Results and discussion

3.1 Time series of trace gas concentrations

Once the humidified clean air is exposed to sunlight, HONO is formed on the chamber walls. Its photolysis increases the concentrations of NO_x and OH (Fig. 1). During this initial phase of the experiment, the OH reactivity is only approximately $1\,s^{-1}$, so that maximum OH concentrations of $1 \times 10^7\,cm^{-3}$ are reached (OH concentrations in Fig. 1 are scaled by a factor of 0.5 during this part of the experiment). MACR injections increase the OH reactivity to up to $13.5\,s^{-1}$, so that OH concentrations drop to (1–1.5) $\times 10^6\,cm^{-3}$. The maximum MACR mixing ratio after the last injection is 14 ppbv. OH dominantly reacts with MACR during the entire experiment (e.g. 14 ppbv MACR corresponds to an OH reactivity of $10\,s^{-1}$). Reaction of OH with MACR initiates a reaction chain that produces RO_2 and HO_2, which includes reactions with NO, so that RO_2 and HO_2 concentrations increase in the presence of MACR. Similarly, concentrations of radical reservoir species peroxyacetyl nitrate and peroxy methacryloyl nitrate, PAN and MPAN (Table 3), are increasing after each MACR injection. These species are products of the reaction of acyl peroxy radicals with NO_2. MPAN and PAN are thermally unstable (Roberts and Bertman, 1992), so that a thermal equilibrium is established. Because PAN is also formed from acetaldehyde in the sunlit chamber, the PAN mixing ratio starts increasing before MACR is injected. The NO concentration is nearly constant over the course of the experiment with a mixing ratio of approximately 90 pptv.

Model calculations applying MCM give OH concentrations, which are approximately 50 % lower than measurements during the MACR oxidation part of the experiment (Fig. 1). The increasing difference between measured and modelled MACR indicates that less MACR is oxidized in the model during the experiment supporting that OH concentrations in the chamber are indeed larger than calculated. The overprediction of MACR would change the OH reactivity by only 10-15 %. This change in the modelled reactivity is not significant.

The decay of measured MACR concentrations can be used to calculate average OH concentrations following the approach described by Poppe et al. (2007). In this approach, the difference of MACR concentrations between two injections is related to the average OH concentrations taking the degradation of MACR by OH and the dilution in the chamber into account. The average OH concentrations required to explain the observed MACR decays are $4 \times 10^6\,\mathrm{cm}^{-3}$, $2.5 \times 10^6\,\mathrm{cm}^{-3}$, and $1.4 \times 10^6\,\mathrm{cm}^{-3}$ between the first and second, second and third, and after the third MACR injection, respectively. This is again consistent with larger measured OH concentrations compared to the modelled OH concentrations.

The reaction of OH with MACR produces three $\mathrm{RO_2}$ species (MCM names: $\mathrm{MACRO2}$, $\mathrm{MACROHO2}$, $\mathrm{MACO3}$, Table 3). Measured $\mathrm{RO_2}$ radical concentrations are reproduced by model calculations. Acyl peroxy radicals like $\mathrm{MACO3}$ are detected by the LIF instrument with low sensitivity (see above). However, the good model-measurement agreement of MPAN and PAN mixing ratios, which are formed from $\mathrm{MACO3}$, indicates that model calculations reproduce $\mathrm{MACO3}$ concentrations. The shape of the temporal behavior of MPAN mixing ratios is determined by the thermal equilibrium between MPAN and $\mathrm{MACO3}$, forcing the fast built up of MPAN after each methacrolein injection. At later times, the concentration of MPAN declines as the production of $\mathrm{MACO3}$ from MACR decreases. $\mathrm{HO_2}$ concentrations are slightly underestimated, but the difference is within the uncertainty of measurements (Table 2).

In general, the description of radical species by the MCM during the part of the experiment before OH reactants are injected into the chamber is expected to be less accurate because: (1) the OH reactivity is mostly caused by unknown species; and (2) radical sources and sinks are not well-defined. After the initial phase of the experiment, the OH reactivity is dominated by MACR. Under these conditions, a much better model-measurement agreement is expected, because chamber specific properties like the small OH reactivity from unknown species do not any longer play a role. This can be seen in similar experiments, when CO or butene was the dominant OH reactant. A model-measurement agreement for radical species within 30 % is achieved in these reference experiments, which are performed on a regular basis in the chamber.

3.2 OH budget analysis

The underprediction of the OH concentration in the model could be caused either by an overestimation of the OH loss or by an underestimation of the OH production. The relatively good agreement of the measured OH reactivity with model calculations (Fig. 1) indicates that an OH source is missing in the model. The missing production rate can be analyzed by a model-independent approach by comparing the OH production and destruction rates of known processes (Hofzumahaus et al., 2009). Primary OH sources in the chamber are O_3 and HONO photolysis. Furthermore, OH is produced from radical recycling via the reaction of HO_2 with NO:

$$O_3 + h\nu \rightarrow O(^1D) + O_2 \tag{R1}$$

$$O(^1D) + H_2O \rightarrow OH + OH \tag{R2}$$

$$HONO + h\nu \rightarrow OH + NO \tag{R3}$$

$$HO_2 + NO \rightarrow OH + NO_2 \tag{R4}$$

All three contributions to the OH production can be calculated using only experimental data. Also the OH reactivity and the OH concentration were measured, so that the OH destruction rate can be calculated. Figure 2 shows time series of the OH production (summed up as coloured areas) and of the OH destruction rate for the experiment on 11 August 2011. Before MACR is injected to the chamber air, the OH production is balanced by its destruction as expected for a short-lived species like OH under steady-state conditions. However, during the MACR oxidation part of the experiment the calculated OH destruction rate is on average twice as large as the sum of OH production from radical recycling via the $HO_2 + NO$ reaction and O_3 and HONO photolysis. As discussed below a potential OH production from the reaction of HO_2 with RO_2 would be small. The grey shaded area in Fig. 2 indicates the additional OH production from an unknown source that is needed to balance the OH destruction ("missing OH source"). Apparently, the missing OH source is linked with the degradation of MACR by OH.

In the following, the data from all experiments are collectively analyzed to determine the missing OH source. This is justified because conditions of the experiments were similar (Table 1). The time-resolved missing OH source shows considerable variability over the course of all experiments, but no significant trend with time is seen in the data (Fig. 3, upper panel). This indicates that the additional OH is most likely not produced from longer-lived first-generation organic products of the MACR oxidation such as hydroxyacetone. These products would accumulate over the course of the experiment because they are less reactive towards OH (Butkovskaya et al., 2006). Therefore, an increasing OH production would be expected, if there was additional OH produced from these species.

Part of the variability of the time series of the missing OH production rate is caused by the variability of the production rate of RO_2 formed in the reaction of MACR with OH (Fig. 3). Here, the RO_2 production rate is calculated from measured OH and MACR concentrations assuming that every reaction of OH with MACR yields one RO_2 radical. Plotting the missing OH production rate against the RO_2 formation rate (Fig. 3) reveals a clear correlation between both values. This suggests that OH is formed from an RO_2 reaction channel missing in the MCM mechanism. The slope of the correlation would be the amount of OH that is additionally produced from each RO_2 radical.

A weighted linear fit with a fixed zero offset gives a value of 0.77 ± 0.31. Here, the 1σ uncertainty of ± 0.31 is determined by the 1σ accuracy of measurements that are included in both coordinates of the correlation (Fig. 3) giving an uncertainty of the slope of approximately $\pm 40\,\%$.

This additional reaction channel competes with the reaction of $\mathrm{RO_2}$ with NO, which finally also regenerates OH, and the reaction of $\mathrm{RO_2}$ with $\mathrm{HO_2}$, which is a radical termination reaction forming peroxides (ROOH):

$$\mathrm{RO_2 + NO \rightarrow RO + NO_2} \tag{R5}$$

$$\mathrm{RO_2 + HO_2 \rightarrow ROOH} \tag{R6}$$

$$\mathrm{RO_2 (+?) \rightarrow OH + products} \tag{R7}$$

Reaction R7 could be either a unimolecular reaction or could involve a reaction partner whose concentration is highly correlated with the $\mathrm{RO_2}$ production. The calculated yield of 0.77 ± 0.31 OH from each $\mathrm{RO_2}$ radical needed to close the OH budget can be regarded as the fractional contribution of Reaction R7 to the $\mathrm{RO_2}$ loss. The large value indicates that this reaction channel is an important pathway for conditions of these experiments (NO mixing ratios less than $100\,\mathrm{pptv}$ and $\mathrm{HO_2}$ concentrations less than $6 \times 10^8\,\mathrm{cm^{-3}}$).

3.3 Modifications of the MACR oxidation scheme

3.3.1 Generic OH recycling with X

A large discrepancy between measured and modelled OH concentrations has been observed in several field campaigns. In order to explain the high OH concentrations in some field campaigns, a generic recycling of OH radicals by a constant amount of an unknown compound X was assumed that would convert peroxy radicals to OH like NO does, but without accompanying ozone production (Hofzumahaus et al., 2009; Lu et al., 2012, 2013):

$$\mathrm{RO_2 + X \rightarrow HO_2} \tag{R8}$$

$$\mathrm{HO_2 + X \rightarrow OH} \tag{R9}$$

Different amounts of X (in units of NO equivalents) were required: Pearl-River-Delta $800\,\mathrm{pptv}$ (Hofzumahaus et al., 2009; Lu et al., 2012), Beijing $400\,\mathrm{pptv}$ (Lu et al., 2013), and Borneo $700\,\mathrm{pptv}$ (Whalley et al., 2011). The nature of X, however, remained unclear, so that this mechanism could only serve as an empirical description. Recently, generic OH recycling was also applied, in order to describe fast OH regeneration from isoprene oxidation by OH in experiments in the SAPHIR chamber (Fuchs et al., 2013). A constant NO equivalent of $100\,\mathrm{pptv}$ was required in this case. It was shown that the effect of a generic OH recycling by X had the same effect as OH production from $\mathrm{RO_2}$ radical isomerization and decomposition reactions.

Generic OH recycling by X is also tested for MACR oxidation experiments here, in order to see, if this empirical mechanism can also describe observations like shown for isoprene oxidation experiments. In fact, all observations including those of OH and MACR can be reproduced, if the mixing ratio of X is assumed to be equivalent to 50 pptv NO (Figs. 4 and 5). This amount of X is only half of what was found for isoprene oxidation for similar conditions (Fuchs et al., 2013) and is approximately ten times smaller compared to the amount of X that was needed to explain the above mentioned field observations.

3.3.2 $\mathbf{RO_2}$ isomerization reactions.

The reaction of OH with MACR either leads to OH addition to the C=C double bond or H-abstraction from the CHO group (Tuazon and Atkinson, 1990; Orlando et al., 1999). OH adds dominantly to the external olefinic carbon atom (yield MCM: 47 %, Fig. 6) forming an $\mathrm{RO_2}$ radical after reaction with $\mathrm{O_2}$ (MCM: $\mathrm{MACRO2}$). OH addition to the internal carbon atom is less likely (yield MCM: 8 %) and forms a different $\mathrm{RO_2}$ radical after reaction with $\mathrm{O_2}$ (MCM: $\mathrm{MACROHO2}$). H-abstraction from the CHO group of MACR leads to the formation of an acyl peroxy radical after reaction with $\mathrm{O_2}$ (MCM: $\mathrm{MACO3}$, yield 45 %, Fig. 6).

Recent work has shown that the yield of OH from the reaction of $\mathrm{HO_2}$ with acyl peroxy radicals like $\mathrm{MACO3}$ could be larger than thought before (Dillon and Crowley, 2008; Taraborrelli et al., 2012). The chemical model MCM used in this work assumes an OH yield of 0.44 for the reaction of $\mathrm{HO_2}$ with $\mathrm{MACO3}$, whereas a yield of <0.7 was found for the simplest acyl peroxy radical $\mathrm{CH_3CO_3}$ (Dillon and Crowley, 2008; Groß, 2014). Although the qualitative behaviour of the missing OH source would be consistent with a larger OH yield from the reaction of $\mathrm{HO_2}$ with $\mathrm{MACO3}$ or other acyl peroxy radicals (Fig. 3), the turnover rates of these reactions are too small, in order to significantly increase the OH production rate. Doubling of the OH yield from the reaction of $\mathrm{MACO3}$ with $\mathrm{HO_2}$ would increase the OH production rate by less than 0.1 $\mathrm{ppbv\,h^{-1}}$ and from the reaction of CH3CO3 with $\mathrm{HO_2}$ less than 0.05 $\mathrm{ppbv\,h^{-1}}$, much smaller than the missing OH production rate.

Quantum chemical calculations showed that $\mathrm{RO_2}$ isomerization with subsequent decomposition could lead to a fast OH regeneration from $\mathrm{RO_2}$ from isoprene via 1,5-H-shift or 1,6-H-shift isomerization with subsequent decomposition of the products (Peeters et al., 2009; Peeters and Müller, 2010; da Silva et al., 2010). Similar reaction schemes have also been proposed for MACR (Peeters et al., 2009; Crounse et al., 2012; Asatryan et al., 2010; da Silva, 2012). A 1,5-H-shift for $\mathrm{MACRO2}$ with subsequent decomposition would produce methylglyoxal, formaldehyde and OH. A rate constant of less than 0.008 $\mathrm{s^{-1}}$ at 303 K has been calculated (Peeters et al., 2009; Crounse et al., 2012). Because additional OH from this isomerization reaction applies only for one $\mathrm{RO_2}$ isomer ($\mathrm{MACRO2}$) from the $\mathrm{OH} + \mathrm{MACR}$ reaction and the rate constant is relatively small, the calculated amount of additional OH produced from this isomerization channel is rather small. Time series of modelled radical and trace gas concentrations are shown in Fig. 4 for this case and Fig. 5 displays the ratio of measured to modelled OH concentrations. The 1,5-H-shift only slightly improves the model-measurement agreement.

In addition to the 1,5-H-shift of $\mathrm{MACRO2}$, a much faster 1,4-H-shift for $\mathrm{MACRO2}$ and a fast 1,5-H-shift for $\mathrm{MACROHO2}$ with an isomerization rate constant of $(0.5 \pm 0.3)\,\mathrm{s}^{-1}$ at $296\,\mathrm{K}$ for both reactions have been suggested (Crounse et al., 2012). The 1,5-H-shift of the aldehyde H-atom in $\mathrm{MACROHO2}$ would produce hydroperoxyacetone (MCM: $\mathrm{HYPERACET}$, Table 3), CO and $\mathrm{HO_2}$. The 1,4-H-shift of $\mathrm{MACRO2}$ would lead to the formation of hydroxyacetone, CO and OH (Crounse et al., 2012) (Fig. 6). A laboratory study (Crounse et al., 2012) shows that hydroxyacetone concentrations, which were measured in MACR oxidation experiments with low NO concentrations, are much larger than expected. According to the study by Crounse et al. (2012) this result is consistent with the fast production of hydroxyacetone in the 1,4-H-shift isomerization channel of $\mathrm{MACRO2}$. Application of a temperature dependence as suggested in literature (Crounse et al., 2012) yields a rate constant of $0.66\,\mathrm{s}^{-1}$ at the temperature during the experiment on 11 August 2011 ($301\,\mathrm{K}$). For conditions of this experiment, more than $95\,\%$ of the $\mathrm{MACRO2}$ would undergo the 1,4-H-shift. Also the branching ratio of the 1,5-H-shift for $\mathrm{MACROHO2}$ would be $95\,\%$, if the reaction rate constant was similarly large as suggested. Figure 4 shows time series of concentrations and Fig. 5 the ratio of measured to modelled OH concentrations (case B), if both, the 1,4-H-shift of $\mathrm{MACRO2}$ and the 1,5-H-shift of $\mathrm{MACROHO2}$, are included. All observations, especially OH concentrations, are matched in this case. Most of the additional OH is formed by the 1,4-H-shift reaction of $\mathrm{MACRO2}$. At the end of the experiment, the isomerization mechanism is expected to increase the hydroxyacetone mixing ratio by $1.5\,\mathrm{ppbv}$ compared to MCM calculations (Fig. 4).

For conditions of these experiments, the ozone production rate is only little less ($< 10\,\%$), when the model modification including the $\mathrm{RO_2}$ isomerization reactions is applied compared to the base case MCM model run. This can be seen in the small changes of the NO mixing ratio and peroxy radical concentrations. The missing contribution of $\mathrm{MACRO2}$ to the ozone production, when isomerization of $\mathrm{MACRO2}$ is the dominant pathway, is partly balanced by the faster production of other $\mathrm{RO_2}$ radicals such as $\mathrm{CH_3O_2}$, which contribute to the ozone production, due to the enhanced OH level. For the same reason, also the ratio of $\mathrm{NO_2}$ to NO mixing ratios does not change much ($< 15\,\%$) between the two models.

Model calculations with variation of the 1,4-H-shift isomerization rate constant were performed to estimate the sensitivity of calculated OH concentrations for experiments here. Decreasing the isomerization rate to a value, for which the median of the difference between measured and modelled OH has a maximum value of $30\,\%$ (the agreement that is expected from reference experiments), gives a lower limit of the rate constant constant of $0.03\,\mathrm{s}^{-1}$. In this case, the $\mathrm{MACRO2}$ isomerization reaction would regenerate $50\,\%$ of the OH radicals that were consumed in the $\mathrm{MACR{+}OH}$ reaction to produce $\mathrm{MACRO2}$. This result is independent of the choice of OH data from either the DOAS or the LIF instrument, because the lower limit is determined by the slightly smaller OH concentrations measured by DOAS compared to LIF (see above). In contrast, modelled OH concentrations are insensitive to a reaction rate constant larger than suggested in literature (Crounse et al., 2012). In this case, $\mathrm{MACRO2}$ and also $\mathrm{MACROHO2}$ radicals nearly exclusively undergo isomerization for conditions of this experiment (Fig. 6). The yield of OH regenerated by isomerization becomes limited by the yields of $\mathrm{MACRO2}$ and $\mathrm{MACROHO2}$ from the reaction of MACR with OH. This implies that the isomerization reaction is much faster than all other reaction of $\mathrm{MACRO2}$ and $\mathrm{MACROHO2}$ for conditions of the experiment. Our OH yield of 0.77 for each OH radical consumed by MACR (Fig. 3) is larger than the yield of 0.55 predicted by the model calculation, if $\mathrm{MACRO2}$ and $\mathrm{MACROHO2}$ is completely converted to OH in the isomerization reaction. This is, however, no contradiction considering the relative large uncertainty of ± 0.3 (1σ) of our experimental value and the uncertainty of the model. Thus, our SAPHIR experiments presented in this work do not allow to determine an upper limit of the 1,4-H-shift isomerization rate constant.

Besides thermal decomposition of $\mathrm{RO_2}$ another reaction scheme has been proposed from quantum-chemical calculations (da Silva, 2012; Asatryan et al., 2010). This suggests that the vibrationally excited adduct of MACR and OH reacts with $\mathrm{O_2}$ on a similar time-scale as collisional deactivation of the adduct takes place. As a consequence, approximately 20 % of the MACR-OH adduct would react with $\mathrm{O_2}$ and would form “double activated” $\mathrm{RO_2}$ radicals, which then can decompose (da Silva, 2012). Decomposition of the “double activated” $\mathrm{RO_2}$ would lead to the formation of either methylglyoxal, formaldehyde and OH or hydroxyacetone, CO and OH. In the result, this mechanism is equivalent to the 1,4- and 1,5-H-shift isomerization reactions (Table 4) and would be equivalent to a maximum isomerization rate constant of $0.007\,\mathrm{s^{-1}}$, in order to yield a branching ratio of maximum 20 % for conditions of these experiments. As shown above, more than 50 % of $\mathrm{MACRO2}$ needs to immediately regenerate OH, in order to explain our observations, much larger than the 20 % yield of “double activated” $\mathrm{RO_2}$. Therefore, this mechanism alone is not sufficient to bring calculations and measurements into agreement. Nevertheless, part of the discrepancy could be potentially due to the decomposition of “double-activated” $\mathrm{RO_2}$, because it is not possible to distinguish both mechanisms in our experiments.

The 1,4-H-shift isomerization rate constant that is required to explain observations from $\mathrm{MACRO2}$ isomerization ($> 0.03\,\mathrm{s^{-1}}$) is equivalent to the reaction of $\mathrm{MACRO2}$ with more than $150\,\mathrm{pptv}$ NO. This value is larger than the amount of X that is needed to describe measured OH concentrations in the “X”-mechanism (see above). In the “X”-mechanism $50\,\mathrm{pptv}$ X is equivalent to an additional $\mathrm{RO_2}$ loss rate of $0.01\,\mathrm{s^{-1}}$. However, in the “X”-mechanism, additional OH is recycled by all $\mathrm{RO_2}$ species, so that the overall impact is larger than that from $\mathrm{MACRO2}$ alone. Therefore, the 1,4-H-shift isomerization rate constant cannot be directly compared to the loss rate of $\mathrm{MACRO2}$ with X in the “X”-mechanism.

4 Summary and conclusions

Measured OH concentrations during MACR oxidation experiments in the atmosphere simulation chamber SAPHIR are underestimated by the MCM by approximately 50 % (NO mixing ratios approximately 90 pptv, HO_2 concentrations approximately $5 \times 10^8\,\mathrm{cm}^{-3}$ and $T = 301\,\mathrm{K}$). The analysis of the OH budget reveals that an additional OH source is required to balance the measured OH destruction rate. Experiments allow to constrain the overall strength of the OH source regardless of the exact chemical mechanism that is responsible for the OH production.

Production of OH from unimolecular isomerization and decomposition reactions of RO_2 radicals (Peeters et al., 2009; Crounse et al., 2012; Asatryan et al., 2010; da Silva, 2012) and the decomposition of double activated RO_2 (Asatryan et al., 2010; da Silva, 2012) give the same products. These mechanisms produce OH from RO_2 without reactions with NO, consistent with observations here. However, only the 1,4-H-shift (Crounse et al., 2012) is fast enough to bring observations and calculations into agreement, whereas the 1,5-H-shift and decomposition of double activated RO_2 only slightly improves the agreement between model calculations and measurements. Model calculations are consistent with the observations within the expected agreement, if the reaction rate constant for the 1,4-H-shift of the RO_2 isomer MACRO2 is faster than $0.03\,\mathrm{s}^{-1}$. In this case, at least 50 % of MACRO2 undergoes the 1,4-H-shift reaction instead of reacting with NO or HO_2 as assumed in the MCM. Thus, the 1,4-H-shift reaction is competitive to the reaction of MACRO2 with 150 pptv NO or even higher NO mixing ratios using the rate constant by Crounse et al. (2012).

A yield of 0.77 ± 0.31 for additionally produced OH is found from the OH budget analysis in these experiments. For unimolecular RO_2 reactions of MACRO2 and MACROHO2 as suggested by Crounse et al. (2012), 0.55 additional OH can be explained. This value is comparable to the overall yield of OH from unimolecular RO_2 reactions produced from isoprene-derived RO_2 (38–45 %) for similar conditions as inferred by Fuchs et al. (2013). However, the impact of these reaction pathways is less for MACR compared to isoprene for two reasons: (1) typical MACR mixing ratios are smaller compared to isoprene, because MACR is a product of isoprene degradation with a yield of less than 30 % (Galloway et al., 2011); (2) its reaction rate constant with OH is 3.5 times smaller, so that the MACR oxidation rate and therefore the production rate of MACR derived RO_2 is smaller; and (3) the total OH production from RO_2 isomerization reactions is limited by the yield of MACRO2 and MACROHO2.

During field campaigns in the Amazonian rainforest, when unexpected large OH was found, isoprene was the dominant OH reactant. Measurements of the sum of MVK and MACR also indicate substantial amounts of MACR (Kubistin et al., 2010). Assuming that at most half of the measured MVK + MACR concentration was MACR, MACR mixing ratios were only 20 % of the mixing ratio of isoprene, when the largest discrepancy between measured and predicted OH was found (Kubistin et al., 2010). Given the smaller reaction rate constant of MACR with OH the contribution of additional OH from MACR oxidation was significant, but most likely much smaller compared to that from isoprene. Because additional OH production from isoprene alone can only explain a smaller part of the entire gap between measured and predicted OH (Fuchs et al., 2013), the contribution of additional OH from MACR derived $\mathrm{RO_2}$ is most likely not large enough to close the remaining gap. During field measurements in China, MACR oxidation played only a minor role (Lou et al., 2010), so that the impact of additional OH recycling from MACR-derived $\mathrm{RO_2}$ is rather small. Nevertheless, results here show that the class of $\mathrm{RO_2}$ isomerization reactions plays an important role at atmospheric conditions with low NO concentrations.

Acknowledgements. This work was supported by the EU FP-7 program EUROCHAMP-2 (grant agreement no. 228335) and by the EU FP-7 program PEGASOS (grant agreement no. 265307). S. Nehr and B. Bohn thank the Deutsche Forschungsgemeinschaft for funding (grant BO 1580/3-1). The authors thank A. Buchholz, P. Schlag, F. Rubach, H.-C. Wu, S. Dixneuf, M. Vietz, P. Müsgen, and M. Bachner for additional measurements during this campaign and technical support. The authors also thank G. da Silva for helpful discussions.

The service charges for this open access publication
have been covered by a Research Centre of the
Helmholtz Association.

References

Asatryan, R., da Silva, G., and Bozelli, J. W.: Quantum chemical study of the acrolein $(\mathrm{CH_2CHCHO})+\mathrm{OH}+\mathrm{O_2}$ reactions, J. Phys. Chem. A, 114, 8302–8311, doi:10.1021/jp104828a, 2010.

Bohn, B., Rohrer, F., Brauers, T., and Wahner, A.: Actinometric measurements of $\mathrm{NO_2}$ photolysis frequencies in the atmosphere simulation chamber SAPHIR, Atmos. Chem. Phys., 5, 493–503, doi:10.5194/acp-5-493-2005, 2005.

Butkovskaya, N. I., Pouvesle, N., Kukui, A., Mu, Y., and Le Bras, G.: Mechanism of the OH-initiated oxidation of hydroxyacetone over the temperature range 236–298 K, J. Phys. Chem. A, 110, 6833–6843, doi:10.1021/jp056345r, 2006.

Carslaw, N., Creasey, D. J., Harrison, D., Heard, D. E., Hunter, M. C., Jacobs, P. J., Jenkin, M. E., Lee, J. D., Lewis, A. C., Pilling, M. J., Saunders, S. M., and Seakins, P. W.: OH and $\mathrm{HO_2}$ radical chemistry in a forested region of north-western Greece, Atmos. Environ., 35, 4725–4737, doi:10.1016/s1352-2310(01)00089-9, 2001.

Crounse, J. D., Paulot, F., Kjaergaard, H. G., and Wennberg, P. O.: Peroxy radical isomerization in the oxidation of isoprene, Phys. Chem. Chem. Phys., 13, 13607–13613, doi:10.1039/C1CP21330J, 2011.

Crounse, J. D., Knap, H. C., Ornso, K. B., Jorgensen, S., Paulot, F., Kjaergaard, H. G., and Wennberg, P. O.: On the atmospheric fate of methacrolein: 1. Peroxy radical isomerization following addition of OH and $\mathrm{O_2}$, J. Phys. Chem. A, 116, 5756–5762, doi:10.1021/jp211560u, 2012.

da Silva, G.: Reaction of methacrolein with the hydroxyl radical in air: incorporation of secondary $\mathrm{O_2}$ addition into the $\mathrm{MACR}+\mathrm{OH}$ master equation, J. Phys. Chem. A, 116, 5317–5324, doi:10.1021/jp303806w, 2012.

da Silva, G., Graham, C., and Wang, Z.-F.: Unimolecular β-hydroxyperoxy radical decomposition with OH recycling in the photochemical oxidation of isoprene, Environ. Sci. Technol., 44, 250–256, doi:10.1021/es900924d, 2010.

Dillon, T. J. and Crowley, J. N.: Direct detection of OH formation in the reactions of $\mathrm{HO_2}$ with $\mathrm{CH_3C(O)O_2}$ and other substituted peroxy radicals, Atmos. Chem. Phys., 8, 4877–4889, doi:10.5194/acp-8-4877-2008, 2008.

Dorn, H.-P., Brandenburger, U., Brauers, T., and Hausmann, M.: A new in-situ laser long-path absorption instrument for the measurement of tropospheric OH radicals, J. Atmos. Sci., 52, 3373–3380, 1995.

Fuchs, H., Hofzumahaus, A., and Holland, F.: Measurement of tropospheric $\mathrm{RO_2}$ and $\mathrm{HO_2}$ radicals by a laser-induced fluorescence instrument, Rev. Sci. Instrum., 79, 084104, doi:10.1063/1.2968712, 2008.

Fuchs, H., Bohn, B., Hofzumahaus, A., Holland, F., Lu, K. D., Nehr, S., Rohrer, F., and Wahner, A.: Detection of $\mathrm{HO_2}$ by laser-induced fluorescence: calibration and interferences from $\mathrm{RO_2}$ radicals, Atmos. Meas. Tech., 4, 1209–1225, doi:10.5194/amt-4-1209-2011, 2011.

Fuchs, H., Dorn, H.-P., Bachner, M., Bohn, B., Brauers, T., Gomm, S., Hofzumahaus, A., Holland, F., Nehr, S., Rohrer, F., Tillmann, R., and Wahner, A.: Comparison of OH concentration measurements by DOAS and LIF during SAPHIR chamber experiments at high OH reactivity and low NO concentration, Atmos. Meas. Tech., 5, 1611–1626, doi:10.5194/amt-5-1611-2012, 2012.

Fuchs, H., Hofzumahaus, A., Rohrer, F., Bohn, B., Brauers, T., Dorn, H.-P., Häseler, R., Holland, F., Kaminski, M., Li, X., Lu, K., Nehr, S., Tillmann, R., Wegener, R., and Wahner, A.: Experimental evidence for efficient hydroxyl radical regeneration in isoprene oxidation, Nat. Geosci., 6, 1023–1026, doi:10.1038/NGEO1964, 2013.

Galloway, M. M., Huisman, A. J., Yee, L. D., Chan, A. W. H., Loza, C. L., Seinfeld, J. H., and Keutsch, F. N.: Yields of oxidized volatile organic compounds during the OH radical initiated oxidation of isoprene, methyl vinyl ketone, and methacrolein under high-$\mathrm{NO_x}$ conditions, Atmos. Chem. Phys., 11, 10779–10790, doi:10.5194/acp-11-10779-2011, 2011.

Groß, C. B. M., Dillon, T. J., Schuster, G., Lelieveld, J., and Crowley, J. N.: Direct kinetic study of OH and O_3 formation in the reaction of $CH_3C(O)O_2$ with HO_2, J. Phys. Chem. A, 118, 974–985, doi:10.1021/jp412380z, 2014.

Guenther, A. B., Jiang, X., Heald, C. L., Sakulyanontvittaya, T., Duhl, T., Emmons, L. K., and Wang, X.: The Model of Emissions of Gases and Aerosols from Nature version 2.1 (MEGAN2.1): an extended and updated framework for modeling biogenic emissions, Geosci. Model Dev., 5, 1471–1492, doi:10.5194/gmd-5-1471-2012, 2012.

Häseler, R., Brauers, T., Holland, F., and Wahner, A.: Development and application of a new mobile LOPAP instrument for the measurement of HONO altitude profiles in the planetary boundary layer, Atmos. Meas. Tech. Discuss., 2, 2027–2054, doi:10.5194/amtd-2-2027-2009, 2009.

Hausmann, M., Brandenburger, U., Brauers, T., and Dorn, H.-P.: Detection of tropospheric OH radicals by long-path differential-optical-absorption spectroscopy: Experimental setup, accuracy, and precision, J. Geophys. Res., 102, 16011–16022, doi:10.1029/97jd00931, 1997.

Hofzumahaus, A., Rohrer, F., Lu, K., Bohn, B., Brauers, T., Chang, C.-C., Fuchs, H., Holland, F., Kita, K., Kondo, Y., Li, X., Lou, S., Shao, M., Zeng, L., Wahner, A., and Zhang, Y.: Amplified trace gas removal in the troposphere, Science, 324, 1702–1704, doi:10.1126/science.1164566, 2009.

Jenkin, M. E., Saunders, S. M., and Pilling, M. J.: The tropospheric degradation of volatile organic compounds: a protocol for mechanism development, Atmos. Environ., 31, 81–104, 1997.

Jordan, A., Haidacher, S., Hanel, G., Hartungen, E., Märk, L., Seehauser, H., Schottkowsky, R., Sulzer, P., and Märk, T. D.: A high resolution and high sensitivity proton-transfer-reaction time-of-flight mass spectrometer (PTR-TOF-MS), Int. J. Mass Spectrom., 286, 122–128, doi:10.1016/j.ijms.2009.07.005, 2009.

Karl, M., Dorn, H. P., Holland, F., Koppmann, R., Poppe, D., Rupp, L., Schaub, A., and Wahner, A.: Product study of the reaction of OH radicals with isoprene in the atmosphere simulation chamber SAPHIR, J. Atmos. Chem., 55, 167–187, doi:10.1007/s10874-006-9034-x, 2006.

Kelly, T. J. and Fortune, C. R.: Continuous monitoring of gaseous formaldehyde using an improved fluorescence approach, Int. J. Anal. Chem., 54, 249–263, 1994.

Kubistin, D., Harder, H., Martinez, M., Rudolf, M., Sander, R., Bozem, H., Eerdekens, G., Fischer, H., Gurk, C., Klüpfel, T., Königstedt, R., Parchatka, U., Schiller, C. L., Stickler, A., Taraborrelli, D., Williams, J., and Lelieveld, J.: Hydroxyl radicals in the tropical troposphere over the Suriname rainforest: comparison of measurements with the box model MECCA, Atmos. Chem. Phys., 10, 9705–9728, doi:10.5194/acp-10-9705-2010, 2010.

Kuhn, U., Andreae, M. O., Ammann, C., Araújo, A. C., Brancaleoni, E., Ciccioli, P., Dindorf, T., Frattoni, M., Gatti, L. V., Ganzeveld, L., Kruijt, B., Lelieveld, J., Lloyd, J., Meixner, F. X., Nobre, A. D., Pöschl, U., Spirig, C., Stefani, P., Thielmann, A., Valentini, R., and Kesselmeier, J.: Isoprene and monoterpene fluxes from Central Amazonian rainforest inferred from tower-based and airborne measurements, and implications on the atmospheric chemistry and the local carbon budget, Atmos. Chem. Phys., 7, 2855–2879, doi:10.5194/acp-7-2855-2007, 2007.

Lelieveld, J., Butler, T. M., Crowley, J. N., Dillon, T. J., Fischer, H., Ganzeveld, L., Harder, H., Lawrence, M. G., Martinez, M., Taraborrelli, D., and Williams, J.: Atmospheric oxidation capacity sustained by a tropical forest, Nature, 452, 737–740, doi:10.1038/nature06870, 2008.

Lindinger, W., Hansel, A., and Jordan, A.: On-line monitoring of volatile organic compounds at pptv levels by means of proton-transfer-reaction mass spectrometry (PTR-MS) – Medical applications, food control and environmental research, Int. J. Mass Spectrom., 173, 191–241, doi:10.1016/s0168-1176(97)00281-4, 1998.

Liu, Y. J., Herdlinger-Blatt, I., McKinney, K. A. and Martin, S. T.: Production of methyl vinyl ketone and methacrolein via the hydroperoxyl pathway of isoprene oxidation, Atmos. Chem. Phys., 13, 5715–5730, doi:10.5194/acp-13-5715-2013, 2013.

Lou, S., Holland, F., Rohrer, F., Lu, K., Bohn, B., Brauers, T., Chang, C.C., Fuchs, H., Häseler, R., Kita, K., Kondo, Y., Li, X., Shao, M., Zeng, L., Wahner, A., Zhang, Y., Wang, W., and Hofzumahaus, A.: Atmospheric OH reactivities in the Pearl River Delta – China in summer 2006: measurement and model results, Atmos. Chem. Phys., 10, 11243–11260, doi:10.5194/acp-10-11243-2010, 2010.

Lu, K. D., Rohrer, F., Holland, F., Fuchs, H., Bohn, B., Brauers, T., Chang, C. C., Häseler, R., Hu, M., Kita, K., Kondo, Y., Li, X., Lou, S. R., Nehr, S., Shao, M., Zeng, L. M., Wahner, A., Zhang, Y. H., and Hofzumahaus, A.: Observation and modelling of OH and HO_2 concentrations in the Pearl River Delta 2006: a missing OH source in a VOC rich atmosphere, Atmos. Chem. Phys., 12, 1541–1569, doi:10.5194/acp-12-1541-2012, 2012.

Lu, K. D., Hofzumahaus, A., Holland, F., Bohn, B., Brauers, T., Fuchs, H., Hu, M., Häseler, R., Kita, K., Kondo, Y., Li, X., Lou, S. R., Oebel, A., Shao, M., Zeng, L. M., Wahner, A., Zhu, T., Zhang, Y. H., and Rohrer, F.: Missing OH source in a suburban environment near Beijing: observed and modelled OH and HO_2 concentrations in summer 2006, Atmos. Chem. Phys., 13, 1057–1080, doi:10.5194/acp-13-1057-2013, 2013.

Orlando, J. J., Tyndall, G. S., Fracheboud, J.-M., Estupiñan, E. G., Haberkorn, S., and Zimmer, A.: The rate and mechanism of the gas-phase oxidation of hydroxyacetone, Atmos. Environ., 33, 1621–1629, doi:10.1016/s1352-2310(98)00386-0, 1999.

Peeters, J. and Müller, J.-F.: HO_x radical regeneration in isoprene oxidation via peroxy radical isomerisations, 2: experimental evidence and global impact, Phys. Chem. Chem. Phys., 12, 14227–14235, doi:10.1039/C0CP00811G, 2010.

Peeters, J., Nguyen, T. L., and Vereecken, L.: HO_x radical regeneration in the oxidation of isoprene, Phys. Chem. Chem. Phys., 11, 5935–5939, doi:10.1039/b908511d, 2009.

Poppe, D., Brauers, T., Dorn, H.-P., Karl, M., Mentel, T., Schlosser, E., Tillmann, R., Wegener, R., and Wahner, A.: OH-initiated degradation of several hydrocarbons in the atmosphere simulation chamber SAPHIR, J. Atmos. Chem., 57, 203–2014, doi:10.1007/s10874-007-9065-y, 2007.

Ren, X., Olson, J. R., Crawford, J. H., Brune, W. H., Mao, J., Long, R. B., Chen, Z., Chen, G., Avery, M. A., Sachse, G. W., Barrick, J. D., Diskin, G. S., Huey, L. G., Fried, A., Cohen, R. C., Heikes, B., Wennberg, P. O., Singh, H. B., Blake, D. R., and Shetter, R. E.: HO_x chemistry during INTEX-A 2004: observation, model calculation, and comparison with previous studies, J. Geophys. Res., 113, D05310, doi:10.1029/2007JD009166, 2008.

Ridley, B. A., Grahek, F. E., and Walega, J. G.: A small, high-sensitivity, medium-response ozone detector suitable for measurements from light aircraft, J. Atmos. Ocean. Tech., 9, 142–148, doi:10.1175/1520-0426(1992)009<0142:ASHSMR>2.0.CO;2, 1992.

Roberts, J. M. and Bertman, S. B.: The thermal decomposition of peroxyacetic nitric anhydride (PAN) and peroxymethacrylic nitric anhydride (MPAN), Int. J. Chem. Kin., 24, 297–307, doi:10.1002/kin.550240307, 1992.

Rohrer, F. and Brüning, D.: Surface NO and $\mathrm{NO_2}$ mixing ratios measured between 30° N and 30° S in the Atlantic region, J. Atmos. Chem., 15, 253–267, 1992.

Rohrer, F., Bohn, B., Brauers, T., Brüning, D., Johnen, F.-J., Wahner, A., and Kleffmann, J.: Characterisation of the photolytic HONO-source in the atmosphere simulation chamber SAPHIR, Atmos. Chem. Phys., 5, 2189–2201, doi:10.5194/acp-5-2189-2005, 2005.

Saunders, S. M., Jenkin, M. E., Derwent, R. G., and Pilling, M. J.: Protocol for the development of the Master Chemical Mechanism, MCM v3 (Part A): tropospheric degradation of non-aromatic volatile organic compounds, Atmos. Chem. Phys., 3, 161–180, doi:10.5194/acp-3-161-2003, 2003.

Schlosser, E., Bohn, B., Brauers, T., Dorn, H.-P., Fuchs, H., Häseler, R., Hofzumahaus, A., Holland, F., Rohrer, F., Rupp, L. O., Siese, M., Tillmann, R., and Wahner, A.: Intercomparison of two hydroxyl radical measurement techniques at the atmosphere simulation chamber SAPHIR, J. Atmos. Chem., 56, 187–205, doi:10.1007/s10874-006-9049-3, 2007.

Schlosser, E., Brauers, T., Dorn, H.-P., Fuchs, H., Häseler, R., Hofzumahaus, A., Holland, F., Wahner, A., Kanaya, Y., Kajii, Y., Miyamoto, K., Nishida, S., Watanabe, K., Yoshino, A., Kubistin, D., Martinez, M., Rudolf, M., Harder, H., Berresheim, H., Elste, T., Plass-Dülmer, C., Stange, G., and Schurath, U.: Technical Note: Formal blind intercomparison of OH measurements: results from the international campaign HOxComp, Atmos. Chem. Phys., 9, 7923–7948, doi:10.5194/acp-9-7923-2009, 2009.

Stone, D., Evans, M. J., Commane, R., Ingham, T., Floquet, C. F. A., McQuaid, J. B., Brookes, D. M., Monks, P. S., Purvis, R., Hamilton, J. F., Hopkins, J., Lee, J., Lewis, A. C., Stewart, D., Murphy, J. G., Mills, G., Oram, D., Reeves, C. E., and Heard, D. E.: $\mathrm{HO_x}$ observations over West Africa during AMMA: impact of isoprene and $\mathrm{NO_x}$, Atmos. Chem. Phys., 10, 9415–9429, doi:10.5194/acp-10-9415-2010, 2010.

Tan, D., Faloona, I., Simpas, J. B., Brune, W., Shepson, P. B., Couch, T. L., Summer, A. L., Carroll, M. A., Thornberry, T., Apel, E., Riemer, D., and Stockwell, W.: $\mathrm{HO_x}$ budget in a deciduous forest: results from the PROPHET summer 1998 campaign, J. Geophys. Res., 106, 24407–24427, 2001.

Taraborrelli, D., Lawrence, M. G., Crowley, J. N., Dillon, T. J., Gromov, S., Grosz, C. B. M., Vereecken, L., and Lelieveld, J.: Hydroxyl radical buffered by isoprene oxidation over tropical forests, Nat. Geosci., 5, 190–193, doi:10.1038/ngeo1405, 2012.

Tuazon, E. C. and Atkinson, R.: A product study of the gas-phase reaction of methacrolein with the OH radical in the presence of $\mathrm{NO_x}$, Int. J. Chem. Kin., 22, 591–602, doi:10.1002/kin.550220604, 1990.

Volz-Thomas, A., Xueref, I., and Schmitt, R.: An automatic gas chromatograph and calibration system for ambient measurements of PAN and PPN, Environ. Sci. Pollut. Res., 4, 72–76, 2002.

Whalley, L. K., Edwards, P. M., Furneaux, K. L., Goddard, A., Ingham, T., Evans, M. J., Stone, D., Hopkins, J. R., Jones, C. E., Karunaharan, A., Lee, J. D., Lewis, A. C., Monks, P. S., Moller, S. J., and

Heard, D. E.: Quantifying the magnitude of a missing hydroxyl radical source in a tropical rainforest, Atmos. Chem. Phys., 11, 7223–7233, doi:10.5194/acp-11-7223-2011, 2011.

Wolfe, G. M., Thornton, J. A., Bouvier-Brown, N. C., Goldstein, A. H., Park, J.-H., McKay, M., Matross, D. M., Mao, J., Brune, W. H., LaFranchi, B. W., Browne, E. C., Min, K.-E., Wooldridge, P. J., Cohen, R. C., Crounse, J. D., Faloona, I. C., Gilman, J. B., Kuster, W. C., de Gouw, J. A., Huisman, A., and Keutsch, F. N.: The Chemistry of Atmosphere-Forest Exchange (CAFE) Model – Part 2: Application to BEARPEX-2007 observations, Atmos. Chem. Phys., 11, 1269–1294, doi:10.5194/acp-11-1269-2011, 2011.

Wolfe, G. M., Crounse, J. D., Parrish, J. D., St. Clair, J. M., Beaver, M. R., Paulot, F., Yoon, T., Wennberg, P. O., and Keutsch, F. N.: Photolysis, OH reactivity and ozone reactivity of a proxy for isoprene-derived hydroperoxyenals, Phys. Chem. Chem. Phys., 14, 7276–7286, doi:10.1039/C2CP40388A, 2012.

Table 1. Experimental conditions of the MACR oxidation experiments. Maximum values are given for MACR and averaged values for the part of the experiment, when MACR was present, for the other parameters.

MACR ppbv	OH $10^6\,\mathrm{cm}^{-3}$	$\mathrm{NO_x}$ ppbv	NO pptv	$\mathrm{O_3}$ ppbv	RH %	$j(\mathrm{NO_2})$ $10^{-3}\,\mathrm{s}^{-1}$	T K	date
14	2.5	0.8	90	40	40	4	301	11 Aug 2011
7	3.5	0.7	60	50	30	4	308	29 Aug 2012
9	3.5	0.6	70	40	45	4.5	302	6 Sep 2012

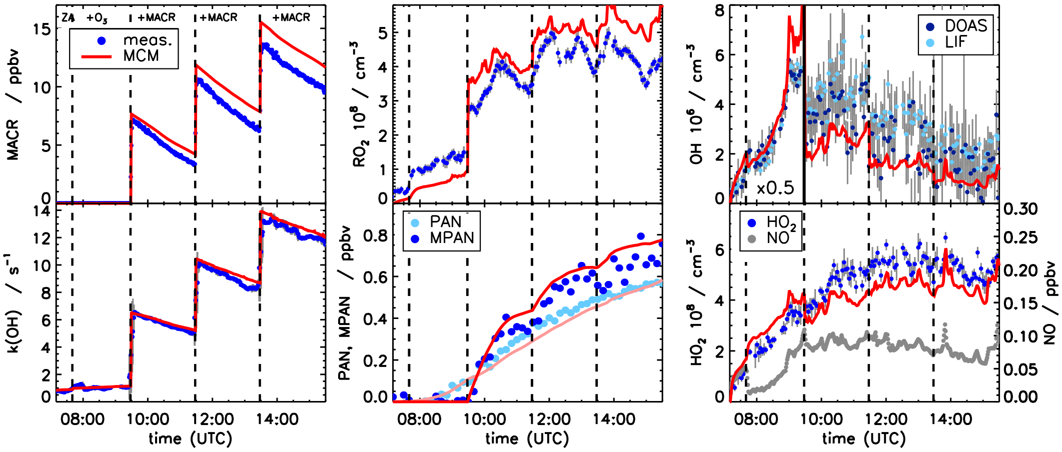

Fig. 1. Measured and modelled time series of MACR, $k(\mathrm{OH})$, PAN, MPAN, $\mathrm{RO_2}$, $\mathrm{HO_2}$, OH and NO for the experiment on 11 August 2011. OH concentrations prior to the addition of MACR ("ZA", "+$\mathrm{O_3}$") are scaled by a factor of 0.5. Model calculations applying MCM underestimate OH concentrations. Measured and modelled $\mathrm{HO_2}$ concentrations include a small fraction of $\mathrm{RO_2}$ radicals, which show up as an interference in the $\mathrm{HO_2}$ detection (less than 5 % of the entire concentration). $\mathrm{RO_2}$ radical concentrations shown here do not include the class of acyl peroxy radicals, which cannot be detected by the instrument.

Table 2. Instrumentation for radical and trace gas detection during the MACR oxidation experiments.

	Technique	Time Resolution	1σ Precision	1σ Accuracy
OH	DOAS[a] (Dorn et al., 1995; Hausmann et al., 1997; Schlosser et al., 2007)	$205\,\mathrm{s}$	$0.8\times10^{6}\,\mathrm{cm^{-3}}$	$6.5\,\%$
OH	LIF[b] (Lu et al., 2012)	$47\,\mathrm{s}$	$0.3\times10^{6}\,\mathrm{cm^{-3}}$	$13\,\%$
$\mathrm{HO_2}$, $\mathrm{RO_2}$	LIF[b] (Fuchs et al., 2011)	$47\,\mathrm{s}$	$1.5\times10^{7}\,\mathrm{cm^{-3}}$	$16\,\%$
k(OH)	Laser-photolysis + LIF[b] (Lou et al., 2010)	$180\,\mathrm{s}$	$0.3\,\mathrm{s^{-1}}$	$0.5\,\mathrm{s^{-1}}$
NO	Chemiluminescence (Rohrer and Brüning, 1992)	$180\,\mathrm{s}$	$4\,\mathrm{pptv}$	$5\,\%$
$\mathrm{NO_2}$	Chemiluminescence (Rohrer and Brüning, 1992)	$180\,\mathrm{s}$	$2\,\mathrm{pptv}$	$5\,\%$
$\mathrm{O_3}$	Chemiluminescence (Ridley et al., 1992)	$180\,\mathrm{s}$	$60\,\mathrm{pptv}$	$5\,\%$
MACR	PTR-TOF-MS[c] (Lindinger et al., 1998; Jordan et al., 2009)	$30\,\mathrm{s}$	$15\,\mathrm{pptv}$	$14\,\%$
HONO	LOPAP[d] (Häseler et al., 2009)	$300\,\mathrm{s}$	$1.3\,\mathrm{pptv}$	$10\,\%$
HCHO	Hantzsch monitor (Kelly and Fortune, 1994)	$120\,\mathrm{s}$	$20\,\mathrm{pptv}$	$5\,\%$
$\mathrm{CH_3CHO}$	PTR-TOF-MS[c] (Lindinger et al., 1998; Jordan et al., 2009)	$30\,\mathrm{s}$	$50\,\mathrm{pptv}$	$15\,\%$
PAN	GC[e] (Volz-Thomas et al., 2002)	$600\,\mathrm{s}$	$25\,\mathrm{pptv}$	$10\,\%$
MPAN	GC[e] (Volz-Thomas et al., 2002)	$600\,\mathrm{s}$	$25\,\mathrm{pptv}$	$20\,\%$
Photolysis frequencies	Spectroradiometer (Bohn et al., 2005)	$60\,\mathrm{s}$	$10\,\%$	$10\,\%$

[a] Differential Optical Absorption Spectroscopy.
[b] Laser Induced Fluorescence.
[c] Proton-Transfer-Reaction Time-Of-Flight Mass-Spectrometry.
[d] LOng Path Absorption Photometer.
[e] Gas Chromatography.

Table 3. Chemical structure of MACR and products from its oxidation with OH. Acronyms are taken from the MCM.

MACR (methacrolein)	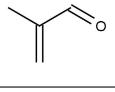
$\mathrm{MACRO2}$	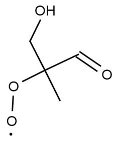
$\mathrm{MACROHO2}$	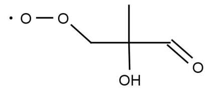
$\mathrm{MACO3}$	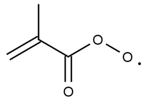
ACETOL (hydroxyacetone)	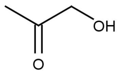
MGLYOX (methylglyoxal)	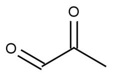
$\mathrm{HYPERACET}$ (hydroperoxyacetone)	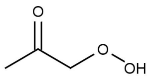
MPAN (peroxy methacryloyl nitrate)	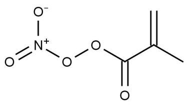
PAN (peroxyacetyl nitrate)	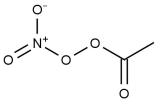

Table 4. Modification of MCM oxidation scheme for MACR. The "X"-mechanism adds generic recycling of OH via reaction of peroxy radicals with a compound X, which behaves like NO. The two cases of $\mathrm{RO_2}$ isomerization produces additional OH via $\mathrm{RO_2}$ isomerization with subsequent decomposition of the products.

	Reaction	Rate constant	Reference
X	$\mathrm{RO_2 + X \rightarrow HO_2}$	$2.7 \times 10^{-12}\exp(360\,\mathrm{K}/T)\,\mathrm{s^{-1}\,cm^3}$	Hofzumahaus et al. (2009)
	$\mathrm{HO_2 + X \rightarrow OH}$	$3.45 \times 10^{-12}\exp(270\,\mathrm{K}/T)\,\mathrm{s^{-1}\,cm^3}$	
$\mathrm{RO_2}$ isom. A	$\mathrm{MACRO2 \xrightarrow{1,5\text{-H-shift}} MGLYOX + OH + HCHO}$	$0.008\,\mathrm{s^{-1}}$	Peeters et al. (2009)
$\mathrm{RO_2}$ isom. B	$\mathrm{MACRO2 \xrightarrow{1,4\text{-H-shift}} ACETOL + OH + CO}$	$2.9 \times 10^{7}\exp(-5300\,\mathrm{K}/T)\,\mathrm{s^{-1}}$	Crounse et al. (2012)
	$\mathrm{MACRO2 \xrightarrow{1,5\text{-H-shift}} MGLYOX + OH + HCHO}$	$0.0018\,\mathrm{s^{-1}}$	
	$\mathrm{MACROHO2 \xrightarrow{1,5\text{-H-shift}} HYPERACET + CO + HO_2}$	$0.5\,\mathrm{s^{-1}}$	

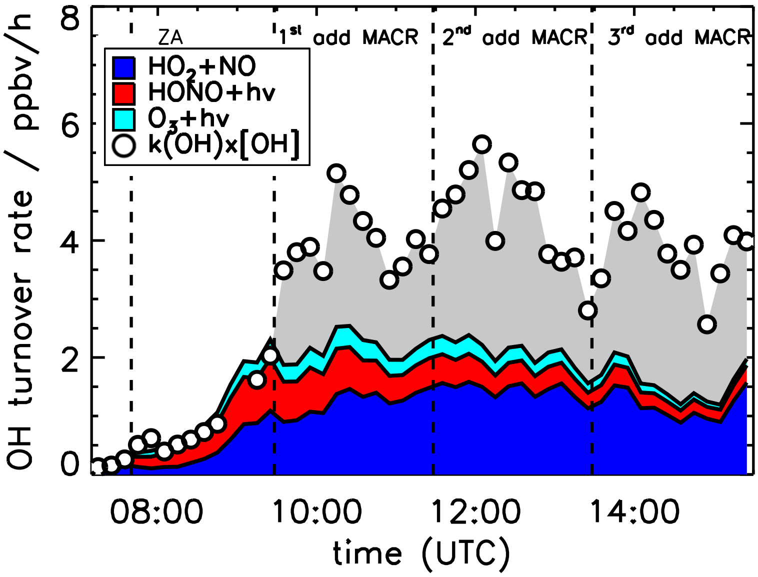

Fig. 2. OH budget for the experiment on 11 August 2011. Black circles give the turnover of the OH destruction rate calculated from measured OH concentrations (DOAS) and the measured OH reactivity. Coloured areas sum up the OH production from sources that can be calculated from measurements. OH production from the reaction of acyl peroxy radicals with HO_2 is negligible here (see discussion). Because of the short lifetime of OH, the production and destruction rates are expected to be equal at all times. The gray area denotes the difference between calculated destruction and production rate. Whereas the OH budget is closed before the injection of MACR ("ZA"), on average half of the OH source is missed during MACR oxidation. HO_2 measurements and calculations include a small interference from specific RO_2 (see text for details).

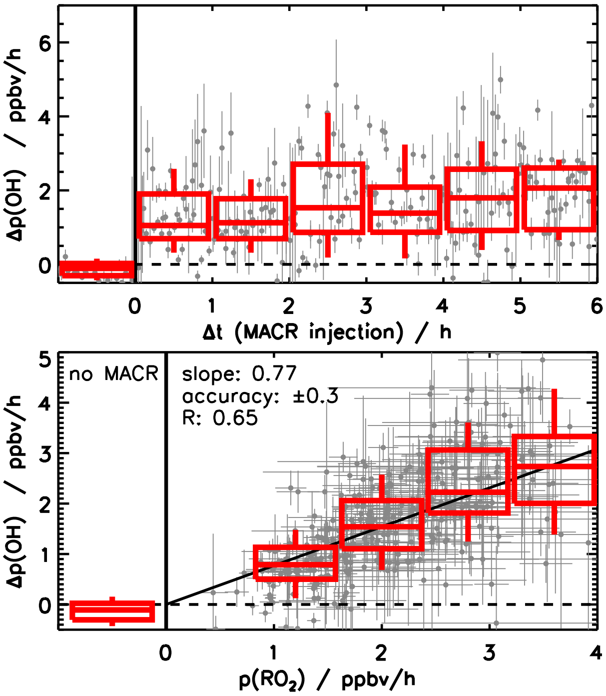

Fig. 3. Scatter plotof the missing OH source ($\Delta p(\mathrm{OH})$) and (1) the time that has elapsed since the first MACR injection (upper panel) and (2) production of $\mathrm{RO_2}$ from the reaction of MACR and OH (lower panel). Grey dots give individual data points with statistical errors for all three experiments (Table 1), boxes show 25 and 75 % and whiskers 10 and 90 % percentiles. The value of the linear correlation coefficient of $R = 0.65$ shows the good correlation between the $\mathrm{RO_2}$ production from MACR and the missing OH source. The slope of a weighted linear fit (black line) suggests that on average 0.77 OH radicals are recycled from $\mathrm{RO_2}$ for conditions of these experiments. The error of 0.3 is calculated from the accuracy of measurements.

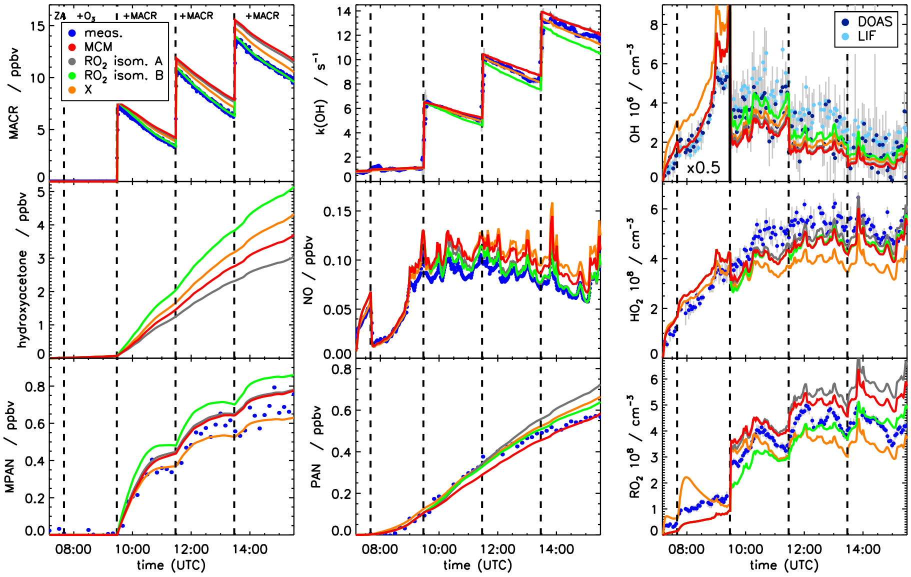

Fig. 4. Measured and modelled time series of MACR, k(OH), PAN, MPAN, RO_2, HO_2, OH and NO for the experiment on 11 August 2011. OH prior to the addition of MACR are scaled by a factor of 0.5. Different model runs were performed applying the MCM, the MCM with two additional RO_2 isomerization reaction schemes (case A and B, see Table 4), and MCM with additional generic OH recycling ("X") with an NO equivalent of 50 pptv. Only calculated hydroxyacetone concentrations are shown, because it was not measured during experiments.

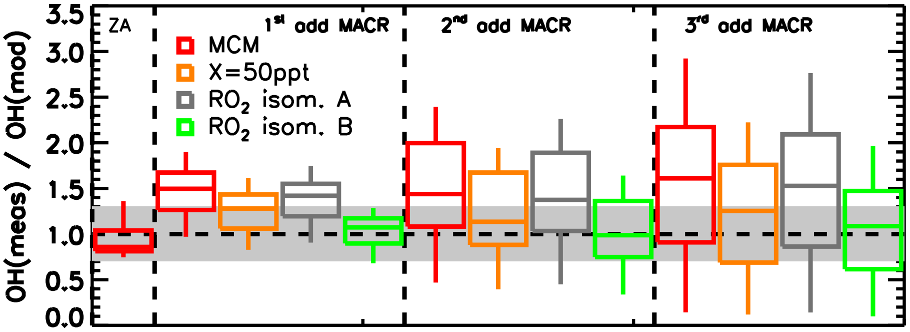

Fig. 5. Ratio of measured (DOAS) to modelled OH concentrations for the four parts of the experiment on 11 August 2011 applying different model approaches: MCM, MCM with additional generic OH recycling ("X"), and MCM with additional RO_2 isomerization schemes (case A and B, see Table 4). The grey shaded area gives the range of agreement of modelled and calculated OH concentrations that is achieved in reference experiments.

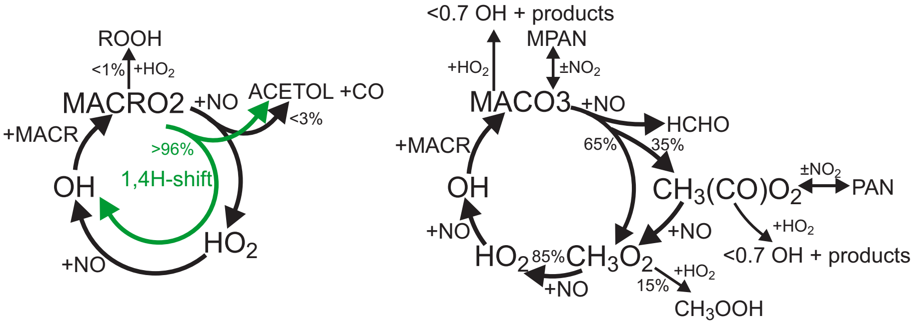

yield: 47%   ***yield: 45%***

Fig. 6. Schematics of radical recycling from the reaction of MACR with OH taken from MCM (black arrows) showing the reactions which were of importance for conditions of these experiments. H-atom abstraction of the CHO group in MACR leads to the formation of an acyl peroxy radical (MACO3: yield 45 %), whereas OH addition to the C=C double bond forms two hydroxyalkoxy radical isomers (RO_2: MACRO2, yield 47 %, and MACROHO2, yield 8 % not shown here). Green arrows indicate the 1,4-H-shift reaction of MACRO2 (Crounse et al., 2012) (the less important 1,5-H-shift is not shown here). Branching ratios are given for conditions of the experiment on 11 August 2011 (NO=90 pptv, $HO_2 = 5 \times 10^8\,cm^{-3}$, $T = 301\,K$), if the fast unimolecular reaction is included.